RSC Advances

PAPER

View Article Online
View Journal | View Issue

Cite this: *RSC Adv.*, 2025, **15**, 51040

Fe-doped MoS_2 monolayers for CO, H_2S, and NO_2 detection: towards advanced environmental sensors

N. V. Hoang *[ab] and Tr. Q. Trieu[c]

In this study, density functional theory (DFT) calculations integrated with machine learning *via* the crystal graph convolutional neural network (CGCNN) were employed to systematically investigate the electronic, magnetic, thermomechanical, and optical properties of Fe-doped MoS_2 (Fe-MoS_2) monolayers before and after the adsorption of CO, H_2S, and NO_2 gas molecules. The computational results reveal that gas adsorption, particularly for CO and NO_2, induces strong interactions with the Fe-MoS_2 surface, leading to pronounced modifications in the electronic band structure, density of states, and charge redistribution. The thermomechanical and optical responses of the system are found to be sensitive to the nature of the adsorbed gas species, with notable variations observed in the elastic moduli and optical absorption coefficients. The Fe-MoS_2 monolayers exhibit strong optical absorption in the ultraviolet to visible spectral range (200–500 nm), alongside tunable electromagnetic characteristics modulated by gas adsorption. These findings highlight the potential of Fe-MoS_2 monolayers as a multifunctional material for applications in gas sensing and optoelectronic devices.

Received 23rd October 2025
Accepted 9th December 2025

DOI: 10.1039/d5ra08121a

rsc.li/rsc-advances

1. Introduction

As electronic and optoelectronic devices continue to advance in intelligence and functionality, the demand for materials with novel and diverse properties becomes increasingly critical. This necessity has driven extensive research into the discovery and design of new materials, with nanomaterials emerging as a particularly promising class. Among the various structural forms under investigation, low-dimensional systems such as monolayers,[1–3] quantum dots,[4–6] quantum wells,[7–9] and quantum wires[10–12] have garnered significant attention due to their unique size-dependent properties.

Monolayer molybdenum disulfide (MoS_2) is a prototypical member of the two-dimensional (2D) transition metal dichalcogenide (TMD) family, structurally analogous to graphene but possessing a semiconducting character. It consists of a single layer of molybdenum (Mo) atoms sandwiched between two layers of sulfur (S) atoms, forming a trigonal prismatic coordination environment (S–Mo–S). Each Mo atom is coordinated by six S atoms, forming a stable hexagonal lattice.[13] While bulk MoS_2 exhibits an indirect band gap of approximately 1.2 eV, the monolayer counterpart undergoes a transition to a direct band gap of about 1.8 eV at the *K* point in the Brillouin zone.[14] This transition significantly enhances its optical activity, rendering monolayer MoS_2 highly attractive for applications in optoelectronic and photonic devices.

The direct band gap of monolayer MoS_2 results in strong photoluminescence (PL) emission in the visible spectrum, along with a pronounced excitonic effect characterized by a high exciton binding energy in the range of 0.5–0.9 eV – substantially greater than that of its bulk form.[15] Furthermore, intrinsic monolayer MoS_2 behaves as an n-type semiconductor, though p-type conduction can be induced through chemical doping or electrostatic gating. The electron mobility in monolayer MoS_2 reaches approximately 200 $cm^2\ V^{-1}\ s^{-1}$ under ambient conditions and can be further enhanced under vacuum or when the monolayer is suspended.[16]

Monolayer MoS_2 can be further functionalized through elemental doping, enabling the formation of novel material systems with enhanced or tailored properties suitable for a broader range of technological applications.[17–19] Among various dopants, transition metal doping has attracted particular interest due to its potential to introduce magnetism and modify electronic characteristics. Using first-principles calculations based on density functional theory (DFT), the structural, electronic, and magnetic properties of a Mn-doped MoS_2 monolayer with the composition $Mo_{0.75}Mn_{0.25}S_2$ have been systematically investigated.[20] The results reveal that the spin-resolved electronic band structure exhibits metallic behavior for the spin-up channel and semiconducting behavior for the spin-down channel, indicating a robust half-metallic nature.

[a]*Atomic Molecular and Optical Physics Research Group, Institute for Advanced Study in Technology, Ton Duc Thang University, Ho Chi Minh City, Vietnam. E-mail: hoangvanngoc@tdtu.edu.vn*

[b]*Faculty of Electrical and Electronics Engineering, Ton Duc Thang University, Ho Chi Minh City, Vietnam*

[c]*Nam Dinh Teacher Training's College, Nam Dinh City, Nam Dinh Province, Vietnam*

This half-metallicity is highly desirable for spintronic applications. The substitutional doping of Mn atoms introduces strong ferromagnetic ordering in the system, which arises from the hybridization between the Mn(3d) orbitals and the Mo(4d) and S(3p) orbitals. To further elucidate the magnetic interactions, the spin-spiral dispersion relation as a function of wave vector was analyzed under generalized Bloch boundary conditions. The exchange coupling parameters $J(i)$ (for $i = 1$–4) were extracted using the Heisenberg model. It was found that the nearest-neighbor exchange interaction $J(1)$ dominates the magnetic coupling, while the next-nearest-neighbor term $J(2)$ also contributes significantly and cannot be neglected. These findings underscore the critical role of both short- and medium-range magnetic interactions in determining the magnetic ground state of Mn-doped MoS_2 monolayers.

In a recent study, DFT was employed to explore the effects of Cr–Mn co-doping at both adjacent and spatially separated lattice sites on the electronic and optical properties of monolayer MoS_2.[21] The computational results demonstrate that co-doping leads to a notable reduction in the band gap and induces a transition from a direct to an indirect band gap semiconductor, accompanied by the emergence of ferromagnetic ordering. Among the configurations considered, spatially separated Cr–Mn doping exhibits the most pronounced effects. From an optical standpoint, the spatially separated Cr–Mn co-doped MoS_2 structure displays significantly enhanced absorption in the visible and ultraviolet regions. This enhancement is accompanied by improved photoelectronic performance, as evidenced by increased optical conductivity, dielectric function components, and absorption coefficients. These findings suggest strong potential for applications in photodetectors, solar energy harvesting devices, and photocatalysis.

In a related investigation, Kumari Prajakta *et al.*[22] conducted a comprehensive DFT analysis of the electronic and optical properties of pristine monolayer MoS_2, MoS_2 containing S/Mo vacancies, and MoS_2 doped with Nb, V, and Zn atoms. The study revealed that pristine MoS_2 exhibits a direct band gap of approximately 1.79 eV, while the doped systems show p-type semiconducting behavior. Optical anisotropy was observed in both the in-plane (x) and out-of-plane (z) directions, particularly in the photon energy range below 11 eV. These results underscore the viability of monolayer MoS_2 and its derivatives as promising candidates for integration into next-generation MOSFET-based nanoelectronic devices.

Surface adsorption studies on monolayer MoS_2 have garnered considerable attention in recent years.[23–25] In one such investigation, Shulin Yang and co-workers employed DFT to examine the adsorption behavior of H_2 molecules on transition metal-doped MoS_2 monolayers.[26] Their findings revealed that Os-doped MoS_2 exhibits the strongest interaction with H_2, characterized by an adsorption energy as low as −1.103 eV. This doped system can stably adsorb up to four H_2 molecules, with an average adsorption energy of approximately −0.792 eV. Furthermore, *ab initio* molecular dynamics simulations confirmed the structural stability of the H_2–Os–MoS_2 complex at 300 K, suggesting its potential applicability for room-temperature hydrogen storage.

In a separate study, Le Li *et al.* utilized first-principles calculations to investigate the adsorption capabilities of elemental mercury (Hg^0) on non-metal-doped MoS_2 monolayers, where the dopants included B, C, N, O, and F.[27] The results indicated that MoS_2 doped with electron-accepting elements such as B, C, and N exhibited stronger adsorption of Hg^0 compared to those doped with isoelectronic (O) or electron-donating (F) elements. A clear trend was observed in which the adsorption strength decreased with increasing valence electron count of the dopant, reaching a critical point at six valence electrons. Among the studied systems, B- and C-doped MoS_2 emerged as the most promising candidates for the effective capture and removal of elemental mercury in environmental pollution control applications.

Numerous recent studies have focused on the physical and chemical properties of MoS_2, driven by its potential for next-generation electronic and sensing applications.[28–31] Among various techniques, stress engineering has emerged as a crucial method for enhancing the electrical performance of semiconductor materials, particularly in silicon-based transistor technologies. In a study by Heechang Shin and colleagues, a biaxial tensile strain engineering strategy was developed for monolayer MoS_2 films synthesized *via* metal–organic chemical vapor deposition (MOCVD).[31] Following the transfer of the MoS_2 film onto a SiO_2/Si substrate, the underlying silicon layer was selectively etched to release compressive stress in the oxide, thereby inducing uniform tensile strain in the overlying MoS_2 monolayer. The magnitude of induced stress was precisely controlled by adjusting the thickness of the stressed oxide layer. Transistors fabricated from these strained MoS_2 films were subsequently transferred onto soft plastic substrates, enabling the maintenance of uniform tensile stress across large areas and paving the way for applications in high-performance, flexible electronic devices.

In the present work, we conduct a comprehensive investigation into the properties of Fe-doped MoS_2 (Fe-MoS_2) monolayers, with particular emphasis on their gas adsorption capabilities. The adsorption behavior of three representative toxic gases – carbon monoxide (CO), hydrogen sulfide (H_2S), and nitrogen dioxide (NO_2) on the Fe-MoS_2 monolayer surface was systematically studied using a combination of DFT and machine learning techniques. This integrated approach provides a powerful framework for both understanding the atomic-scale mechanisms of gas adsorption and accelerating the prediction of material performance across diverse doping and adsorption configurations. The overarching aim is to elucidate the fundamental electronic and adsorption properties of Fe-MoS_2 monolayers and their interactions with gas molecules, thereby informing the design and optimization of materials for future applications in optoelectronic devices and chemical sensing technologies.

Among various transition metals, Fe was selected as the dopant in this study due to its unique ability to induce magnetic moments in non-magnetic 2D materials, particularly MoS_2. This property is essential for potential spintronic and magneto-electronic applications. Furthermore, Fe atoms can effectively hybridize with the MoS_2 lattice, leading to localized states near

the Fermi level that may enhance surface reactivity toward gas molecules. Compared to heavier or more noble transition metals (such as Pd, Pt, or Au), Fe also offers advantages in terms of abundance, lower cost, and environmental compatibility, making it a promising candidate for scalable applications. This work aims to explore the dual roles of Fe in modulating both the magnetic and adsorption properties of MoS_2 monolayers.

2. Methods

The adsorption energy is calculated as follows:[32]

$$E_a = E_t - E_p - E_{gas}$$

where, E_t, E_p, E_{gas} are respectively the total energy of the CO/H_2S/NO_2 adsorption system, the pristine system and of the isolated gas.

2.1. DFT calculations

First-principles calculations based on DFT were conducted using the Quantum ESPRESSO package to investigate the structural, electronic, and optical properties of Fe-doped monolayer MoS_2 (Fe-MoS_2), both in the pristine state and upon adsorption of CO, H_2S, and NO_2 gas molecules. The generalized gradient approximation (GGA) with the Perdew–Burke–Ernzerhof (PBE) functional was employed to describe the exchange–correlation interactions, together with ultrasoft pseudopotentials. A kinetic energy cutoff of 50 Ry and a charge density cutoff of 500 Ry were used throughout the calculations.

A 4×4 supercell with a vacuum region of 20 Å along the out-of-plane direction was constructed to model the monolayer system. Brillouin zone sampling was performed using an $11 \times 11 \times 1$ Monkhorst–Pack k-point grid. Structural relaxations were carried out until the forces on all atoms were less than 10^{-3} Ry bohr^{-1} and the total energy change was below 10^{-6} Ry.

To properly account for dispersion interactions, which play a crucial role in physisorption, Grimme's DFT-D3 van der Waals correction was included in all total-energy and geometry optimization steps. Spin-polarized calculations were performed for all systems to capture magnetic effects induced by Fe doping and gas adsorption. The magnetic parameters were set using $n_{spin} = 2$, and the initial magnetic moment of the Fe dopant was defined through starting_magnetization(i) (with i corresponding to the Fe species). A commonly employed value of starting_magnetization = 0.5 was used to initiate spin polarization. Total and site-resolved magnetic moments were extracted from the self-consistent field (SCF) outputs.

2.2. CGCNN predictions

Thermo-mechanical properties – including bulk and shear moduli, heat capacities, Debye temperature, and thermal expansion coefficients – were predicted using the Crystal Graph Convolutional Neural Network (CGCNN). The model was trained on the Materials Project database, while the optimized DFT structures served as inputs for property inference.

The dataset was divided using an 80 : 20 training–testing ratio and evaluated through 5-fold cross-validation to ensure strong generalization performance. Training was performed with a learning rate of 0.01, a batch size of 256, and a maximum of 150 epochs. The learning objective was to minimize the mean absolute error (MAE), which converged to values below 0.12 eV for the targeted mechanical and thermodynamic property predictions.

3. Results and discussion

3.1. Stability results

Table 1 presents the adsorption energies (E_a) at various adsorption sites for the three gas molecules (CO, H_2S, NO_2) on the Fe-doped MoS_2 monolayer surface. For all three molecules, the lowest adsorption energy is consistently observed at the hollow site. Specifically, the adsorption energies at this site are −1.82 eV for CO, 2.51 eV for H_2S, and −1.62 eV for NO_2, respectively. Therefore, the hollow-site configurations are selected for subsequent calculations of electronic, magnetic, thermo-mechanical, and optical properties in this study. Both CO and NO_2 exhibit negative adsorption energies, indicating exothermic and thermodynamically favorable adsorption processes. Conversely, the H_2S-adsorbed configuration yields a positive adsorption energy, implying that the interaction between H_2S and the Fe-MoS_2 surface is energetically unfavorable under ambient conditions.

Fig. 1 illustrates the optimized atomic configurations of the pristine Fe-doped MoS_2 (Fe-MoS_2) monolayer and the corresponding structures following the adsorption of CO, H_2S, and NO_2 gas molecules. The Fe-MoS_2 monolayer exhibits a hexagonal lattice composed of three atomic layers, with a central transition metal layer (Mo/Fe) sandwiched between two sulfur layers. The key structural parameters of the pristine and gas-adsorbed configurations are summarized in Table 2. Upon gas adsorption, noticeable distortions are observed in the local atomic environment surrounding the Fe dopant site. Specifically, the interatomic distances labeled as d_1, d_2, and d_3 exhibit slight elongations, indicative of localized lattice expansion. Among the studied systems, H_2S adsorption induces the most pronounced structural distortion, with $d_2 = 2.430$ Å, $d_2 = 3.225$ Å, and $d_3 = 3.079$ Å. In contrast, the CO- and NO_2-adsorbed configurations exhibit relatively minor structural perturbations, suggesting weaker lattice coupling.

Magnetic property analysis reveals that the pristine Fe-MoS_2 monolayer possesses a net magnetic moment of $1.9878\mu_B$. Upon adsorption of CO and H_2S, the magnetic moments change only

Table 1 Adsorption energy values at different sites of the configurations

Gas molecules	Top (eV)	Bridge (eV)	Valley (eV)	Hollow (eV)
CO	−1.21	−1.43	−1.37	−1.82
H_2S	3.53	3.22	3.86	2.51
NO_2	−1.02	−1.25	−1.18	−1.62

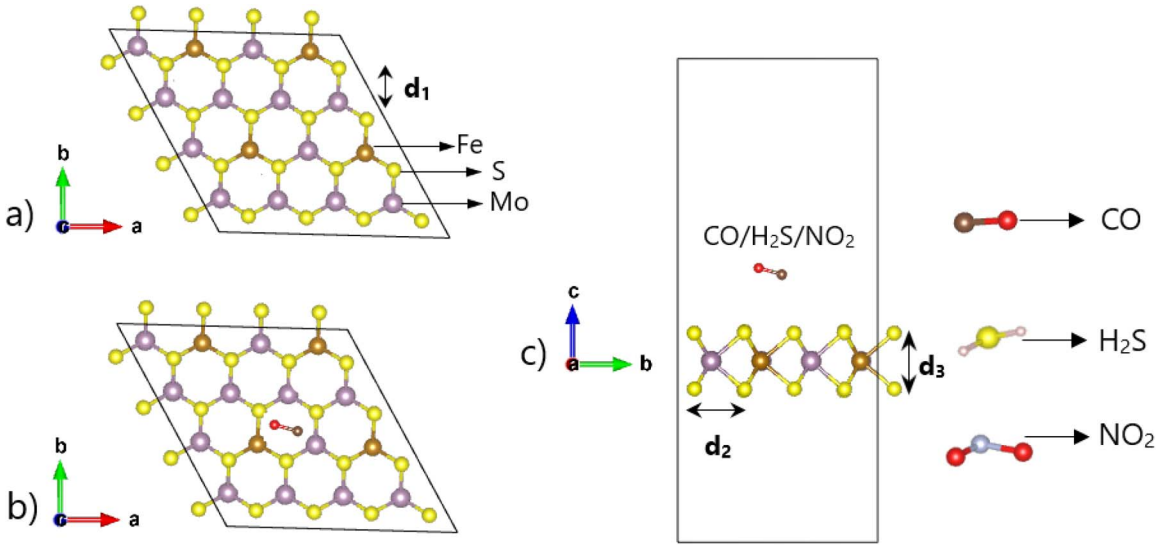

Fig. 1 Top view of the pristine Fe-MoS_2 monolayer (a), top view and side view of the gas-adsorbed Fe-MoS_2 configurations (b and c).

Table 2 Structural parameters of Fe-MoS_2 monolayer and gas adsorption configurations of Fe-MoS_2 monolayer (d_1 is the distance between Mo and S atoms in the hexagon, d_2 is the distance between two S atoms in the same plane, d_3 is the distance between two S atoms in two different planes, μ is the magnetic moment in a unit cell)

Configurations	d_1 (Å)	d_2 (Å)	d_3 (Å)	μ (μ_B)
Pristine Fe-MoS_2	2.415	3.192	3.121	1.9878
CO adsorption	2.420	3.215	3.090	1.9865
H_2S adsorption	2.430	3.225	3.079	2.0447
NO_2 adsorption	2.425	3.219	3.096	0.7576

marginally to 1.9865μ_B and 2.0447μ_B, respectively, indicating negligible perturbation of the spin distribution. However, NO_2 adsorption leads to a substantial reduction in the magnetic moment, decreasing to 0.7576μ_B. This significant drop suggests strong hybridization between the electronic states of NO_2 and the Fe-MoS_2 system, resulting in pronounced suppression of spin polarization.

In previous studies, pristine monolayer MoS_2 has been reported to interact weakly with common gas molecules such as CO, NO_2, and H_2S, typically exhibiting adsorption energies of only a few hundred meV (physisorption). Consequently, the undoped MoS_2 substrate generally shows weak adsorption behavior. This trend was clearly demonstrated in the DFT investigation by Yue *et al.*, where molecules such as CO and NO_2 exhibited small adsorption energies (≈0.1–0.3 eV) on pristine MoS_2.[35] The introduction of dopants or defects significantly enhances the surface reactivity; several reports have shown that both transition-metal doping and sulfur vacancies increase adsorption strength through the formation of localized d-states and stronger orbital hybridization between the dopant and gas molecules.[36,37] Specifically, studies on metal-doped MoS_2 systems (*e.g.*, Ni-, Co-, and Fe-doped MoS_2) have reported substantially larger adsorption energies (up to ~1 eV or higher) for molecules such as H_2S and NO_2, consistent with a chemisorption mechanism arising from strong interactions between the metal d-orbitals and the molecular orbitals.[36,38] Our results – CO ($E_a \approx -1.82$ eV) and NO_2 ($E_a \approx -1.62$ eV) at the hollow site – are in agreement with the enhanced adsorption commonly observed in transition-metal-doped MoS_2 systems and fall well above the typical range for pristine MoS_2. This indicates that Fe doping robustly promotes chemisorption, consistent with previous findings on TM-doped MoS_2.[37,39]

Regarding electronic and magnetic properties, numerous prior studies have demonstrated that transition-metal dopants (including Fe) can introduce d-states near the Fermi level, induce spin splitting, and even convert nonmagnetic semiconductors into spin-polarized semimetals. The results obtained in this work – the emergence of spin-polarized semimetallicity in the pristine-doped system and the transition to fully metallic behavior accompanied by a strong reduction of the magnetic moment upon NO_2 adsorption – are consistent with earlier DFT analyses on the effects of doping and defects on the band structure and magnetism of MoS_2.[38,39]

To comprehensively assess the thermomechanical properties of the material systems, key parameters including bulk modulus (B), shear modulus (G), heat capacity at constant pressure (C_P), heat capacity at constant volume (C_V), Debye temperature (T_D), and thermal expansion coefficient (α) were predicted for the pristine Fe-MoS_2 monolayer and the corresponding gas-adsorbed configurations (CO, H_2S, and NO_2) using the Crystal Graph Convolutional Neural Network (CGCNN) deep learning framework. CGCNN is a graph-based convolutional neural network architecture that encodes the crystal structure as a graph, enabling efficient extraction of local and global structural features and accurate prediction of physical properties.

The predicted values are summarized in Table 3 and reveal notable changes in several thermomechanical characteristics upon gas adsorption. The bulk modulus of the pristine configuration was calculated to be 25.82 GPa, which is significantly

Table 3 Thermo-mechanical parameters of the configurations

Configurations	B (GPa)	G (GPa)	C_P (k_B per atom)	C_V (k_B per atom)	T_D (K)	α (K^{-1})
Pristine Fe-MoS_2	25.82	21.73	2.84	2.77	395.86	6.12×10^{-5}
CO adsorption	33.85	21.40	2.79	2.77	335.17	6.09×10^{-5}
H_2S adsorption	26.69	9.01	2.88	2.79	362.00	6.04×10^{-5}
NO_2 adsorption	32.49	15.99	2.79	2.78	354.71	6.09×10^{-5}

lower than that of bulk MoS_2 (~50.86 GPa (ref. 33)), yet consistent with the expected behavior of a doped two-dimensional material. Upon gas adsorption, the bulk modulus increases markedly for the CO- and NO_2-adsorbed systems, reaching 33.85 GPa and 32.49 GPa, respectively. This increase indicates enhanced volumetric stiffness, likely attributed to the strong chemical interaction between the adsorbed molecules and the Fe-MoS_2 surface, which locally reinforces the lattice structure. In contrast, H_2S adsorption results in only a marginal change (B = 26.69 GPa), remaining close to the pristine value, consistent with a relatively weaker interaction in terms of elastic response.

The shear modulus G exhibits more pronounced variations, highlighting the anisotropic nature of the mechanical response in the 2D system. For the pristine Fe-MoS_2 monolayer, G is calculated to be 21.73 GPa, lower than the bulk value of MoS_2 (46.76 GPa (ref. 33)), as expected for atomically thin structures. Following gas adsorption, G remains nearly unchanged for CO (21.40 GPa), decreases moderately for NO_2 (15.99 GPa), and decreases significantly in the case of H_2S adsorption, dropping to just 9.01 GPa – approximately 41% of the pristine value. This substantial reduction in shear modulus suggests a severe weakening of the material's shear strength upon H_2S adsorption, which aligns with the large structural deformation observed in the geometric analysis. These results indicate that different gas adsorption scenarios can modulate the mechanical resilience of Fe-MoS_2 to varying degrees, with H_2S exerting the most detrimental effect.

To evaluate the consistency and reliability of machine learning predictions, the bulk modulus (B) and shear modulus (G) of the pristine Fe-MoS_2 monolayer were independently calculated using DFT methods, yielding values of 24.31 GPa and 20.26 GPa, respectively. These results are in close agreement with the corresponding values predicted by the CGCNN model, which produced B = 25.82 GPa and G = 21.73 GPa. The relative deviation between the DFT and CGCNN results is less than 7%, confirming that the CGCNN model provides quantitatively reliable estimates of the elastic properties for this system. This agreement validates the application of CGCNN as a complementary and efficient approach for large-scale screening of mechanical properties in doped two-dimensional materials.

From a thermal perspective, both the isobaric heat capacity (C_P) and isochoric heat capacity (C_V) per atom remain relatively stable across all configurations, fluctuating within a narrow range of 2.77–2.88k_B per atom. Among them, the H_2S-adsorbed configuration exhibits the highest C_P value (2.88k_B per atom), which can be attributed to increased vibrational amplitudes arising from structural deformation. Nevertheless, the variation in heat capacity values is minor, suggesting that the overall heat storage capacity of the Fe-MoS_2 system is not significantly affected by gas adsorption.

The Debye temperature (T_D), a key parameter reflecting lattice vibrational stiffness and thermal stability, offers further insight into the thermal behavior of the material. Compared to the T_D of bulk MoS_2 (~278.35 K (ref. 33)), the pristine Fe-MoS_2 monolayer displays a substantially higher value (395.86 K), indicating lattice stiffening induced by Fe doping. Upon gas adsorption, T_D decreases across all configurations, with values of 335.17 K (CO), 354.71 K (NO_2), and 362.00 K (H_2S), suggesting a softening of the vibrational network due to gas–surface interactions. Despite these reductions, all T_D values remain above that of bulk MoS_2, indicating that the Fe-MoS_2 monolayer retains good thermal stability even after gas adsorption.

Finally, the thermal expansion coefficient (α) remains nearly constant across the studied systems, ranging from 6.04×10^{-5} K^{-1} to 6.12×10^{-5} K^{-1}. These values are in close agreement with the reported thermal expansion coefficient of monolayer MoS_2 ($\alpha \approx 6.49 \times 10^{-5}$ K^{-1} (ref. 34)). This consistency suggests that gas adsorption does not significantly alter the material's macroscopic thermal expansion behavior, although localized lattice distortions are evident at the adsorption sites.

As CGCNN directly learns atomic and bonding environments from the crystal graph, the model captures local structural features that govern thermo-mechanical responses. Across all predicted properties – including bulk modulus (B), shear modulus (G), heat capacities (C_P, C_V), Debye temperature (T_D), and thermal expansion coefficient (α) – the model consistently assigned higher importance to the atomic environment surrounding the Fe dopant and the neighboring S atoms. Key features such as bond lengths, local coordination, and atomic connectivity were found to strongly influence the predictive performance, reflecting their critical role in determining lattice stiffness, vibrational behavior, and anharmonic effects. This result underscores the physical interpretability of CGCNN in modeling doped 2D systems and highlights its ability to learn chemically meaningful representations for complex property prediction.

3.2. Electronic results

The electronic band structures and total density of states (TDOS) of the pristine Fe-MoS_2 monolayer and its gas-adsorbed configurations (CO, H_2S, and NO_2) are presented in Fig. 2. As illustrated, the pristine Fe-MoS_2 system, as well as the CO- and H_2S-adsorbed structures, exhibit spin-polarized semimetallic

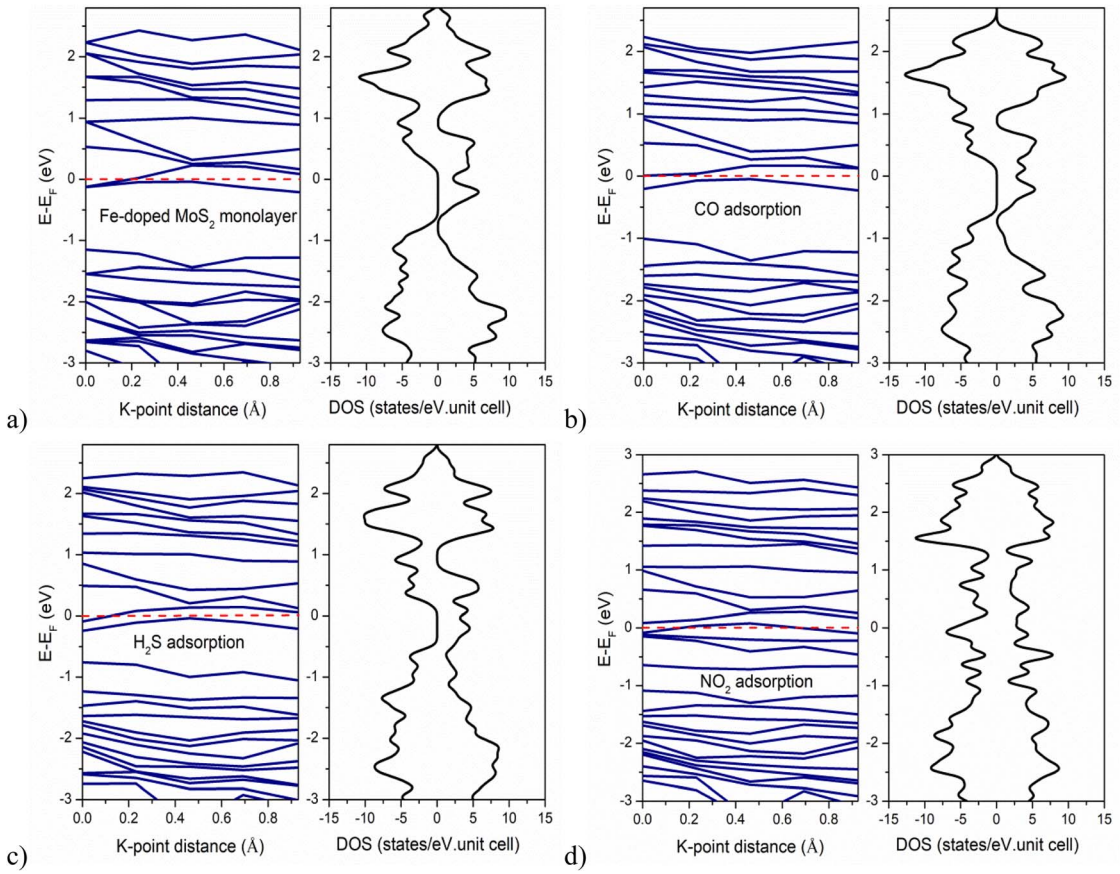

Fig. 2 Energy band structure and total density of states in the structures: Fe-MoS_2 (a), CO adsorption (b), H_2S adsorption (c), NO_2 adsorption (d).

behavior in which the spin-up channel displays metallic characteristics while the spin-down channel retains semiconducting features. In contrast, the NO_2-adsorbed configuration shows metallic behavior in both spin channels, indicating strong electronic hybridization between the NO_2 molecular orbitals and the Fe-MoS_2 substrate. For pristine Fe-MoS_2, the TDOS reveals finite states around the Fermi level, suggesting that Fe doping introduces additional electronic states primarily originating from Fe–S hybridization, thereby reducing the effective bandgap and enhancing carrier availability. Upon gas adsorption, the TDOS becomes noticeably modified, particularly for NO_2. The pristine, CO-, and H_2S-adsorbed structures show no TDOS at the Fermi level in the spin-down channel, whereas distinct TDOS contributions appear around the Fermi level for both spin channels in the NO_2-adsorbed configuration. This confirms that NO_2 induces the strongest electronic perturbation among the examined gases and significantly alters the spin-dependent electronic structure of Fe-MoS_2.

Pristine monolayer MoS_2 and bulk MoS_2 are both spin-unpolarized semiconductors, possessing direct and indirect band gaps of approximately 1.8 eV and 1.2 eV, respectively.[14] The emergence of spin polarization and metallicity in the Fe-doped systems underscores the critical role of Fe dopants in tailoring the electronic structure, enabling modulation of both the magnetic and conductive properties of the material.

Adsorption on the Fe-MoS_2 monolayer caused distinct shifts in the Fermi level (E_F), which was initially calculated at −1.6877 eV. Upon gas exposure, two primary interaction mechanisms were confirmed. Firstly, CO adsorption and NO_2 adsorption both resulted in an upward E_F shift, the E_F moved to −1.6371 eV for CO (a shift of +0.0506 eV) and −1.6099 eV for NO_2 (a shift of +0.0778 eV). In contrast, H_2 adsorption led to a marginal downward E_F shift to −1.6972 eV (a shift of −0.0095 eV). The magnitude and direction of these E_F shifts directly correlate with the induced change in carrier concentration, predicting that NO_2 and CO interactions will yield the highest sensor response due to the substantial alteration of the electronic structure.

Fig. 3 illustrates the state contributions of individual atoms in the Fe-MoS_2 structures and their gas-adsorbed configurations. For the pristine structure (Fig. 3a), Mo, S, and Fe atoms collectively contribute to the TDOS, with S dominating the low-energy region and Mo–Fe contributing significantly near the Fermi level. Upon CO adsorption (Fig. 3b), O atoms exhibit substantial contributions across multiple energy regions, while the contribution of C is mainly localized around −4.5 eV and 1.5 eV, reflecting the hybridization between the CO molecule and the Fe-MoS_2 surface. For H_2S adsorption (Fig. 3c), H atoms contribute only minimally to the TDOS, whereas the S atoms from both the molecule and the substrate dominate the spectral

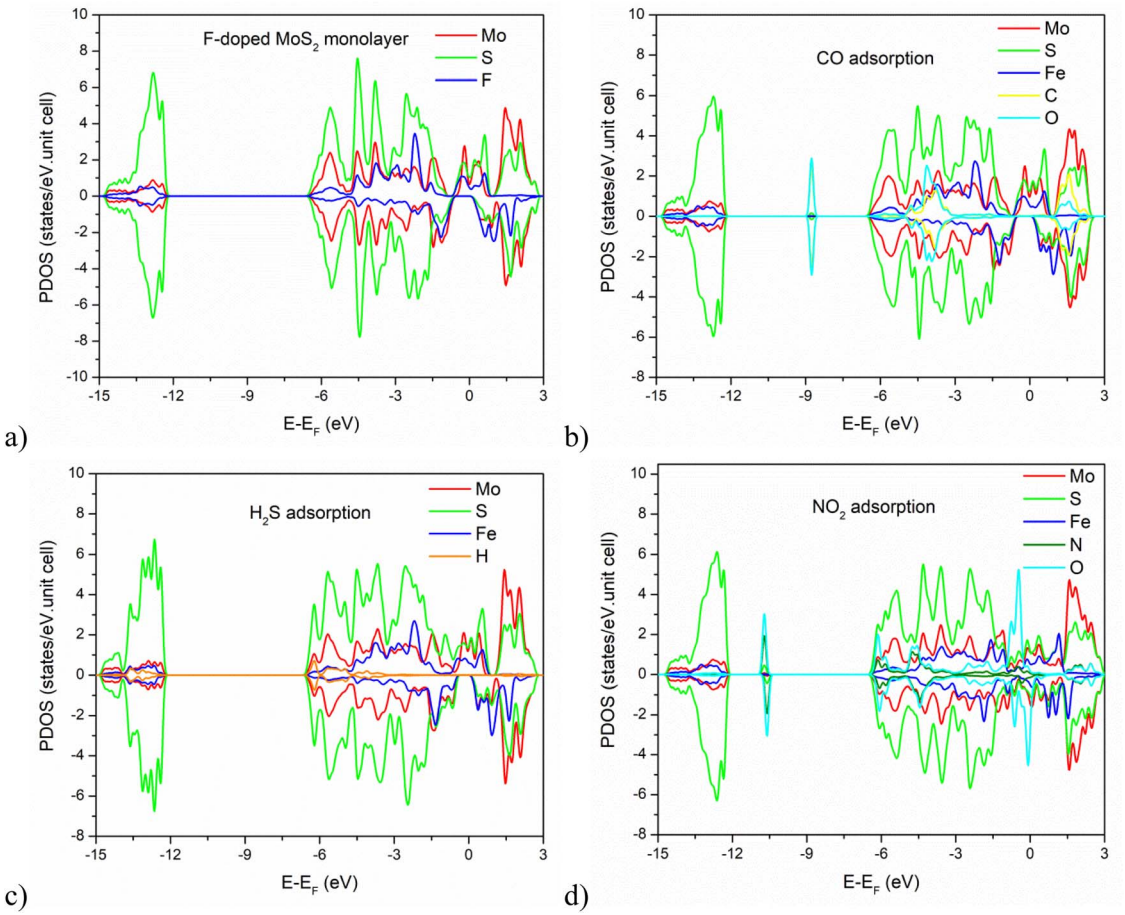

Fig. 3 The state contributions of individual atoms in the structures: Fe-MoS_2 (a), CO adsorption (b), H_2S adsorption (c), NO_2 adsorption (d).

features, indicating a weaker interaction compared to CO. In contrast, the NO_2-adsorbed configuration (Fig. 3d) shows significant contributions from O atoms near the Fermi level, while the contribution from N is much smaller, which partially accounts for the metallic behavior observed in the NO_2-adsorbed structure.

The partial density of states (PDOS) profiles of pristine and gas-adsorbed Fe-MoS_2 (Fig. 4) reveal observable changes in the orbital contributions of Mo, Fe, and S atoms upon adsorption of CO, H_2S, and NO_2. Although these variations are not large, they provide useful insights into the electronic interactions between the gas molecules and the substrate.

A notable feature observed in all gas-adsorbed configurations is the pronounced reduction in the intensity of the Mo(5s) peak. In the pristine Fe-MoS_2 structure, a sharp Mo(5s) peak appears near −4.5 eV; however, upon adsorption of CO, H_2S, or NO_2, the magnitude of this peak decreases significantly.

The sulfur-derived S(3s) and S(3p) states also exhibit reduced spectral intensity after gas adsorption, indicating that S atoms in the MoS_2 lattice participate in electron redistribution upon binding. This depletion arises from hybridization between S orbitals and the constituent atoms of the incoming molecules, signifying perturbation of the valence-band bonding network.

The Fe(4s) states decrease substantially from ∼0.21 states per eV in the pristine configuration to 0.10, 0.14, and 0.09 states per eV for the CO-, H_2S-, and NO_2-adsorbed structures, respectively. This reduction confirms that Fe acts as an active site mediating electronic coupling between the adsorbates and the MoS_2 lattice, and highlights the essential role of Fe doping in enhancing gas sensitivity.

For the CO-adsorbed configuration, the electronic states associated with C and O near −8.9 eV, −4 eV, and +1.8 eV overlap significantly with Mo(5s), Fe(4s), and S(3p) states. This clear orbital alignment is characteristic of chemisorption, producing strong hybridization and considerable charge redistribution at the interface.

In the case of H_2S adsorption, the broad distribution of H-derived molecular states indicates weak and delocalized hybridization. Unlike CO, the frontier orbitals of H_2S couple inefficiently with Mo and Fe due to their lower reactivity and unfavorable symmetry. This weaker coupling explains both the unfavorable (positive) adsorption energy and the limited PDOS perturbation. The accompanying structural distortions and the reduction in shear modulus G further suggest that H_2S disrupts the lattice mechanically rather than forming strong chemical bonds.

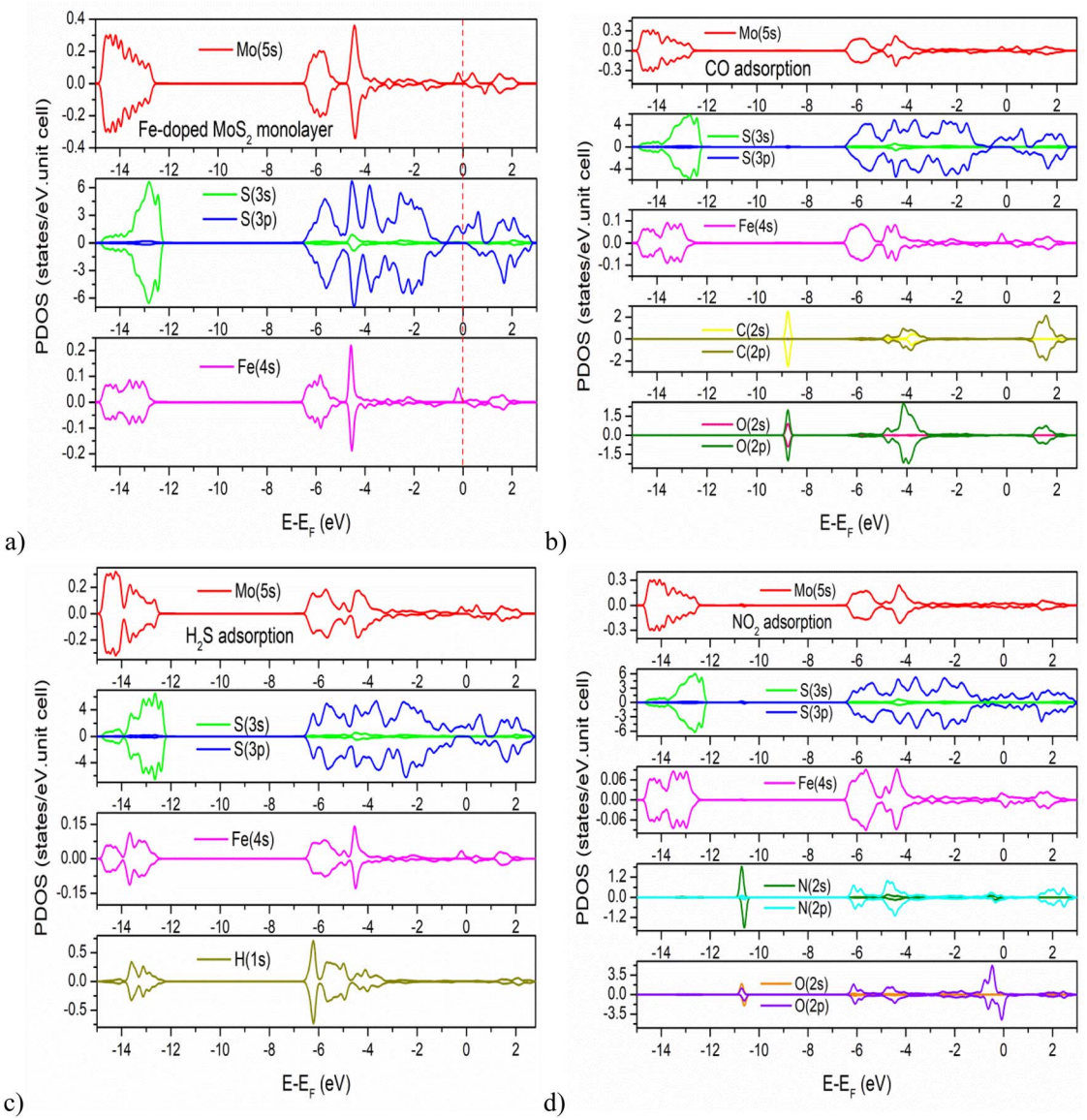

Fig. 4 Partial density of states of the pristine Fe-MoS_2 monolayer structure (a) and the Fe-MoS_2 monolayer structures adsorbed with gases: CO (b), H_2S (c), NO_2 (d).

For NO_2 adsorption, substantial hybridization occurs from −7 eV to +3 eV, where N- and O-derived states strongly overlap with Mo, Fe, and S orbitals. This interaction leads to significant charge redistribution and the observed suppression of the magnetic moment. The strong coupling between NO_2 and the substrate is fully consistent with its chemisorption behavior, driven by the high electronegativity of the molecule.

The charge density difference (CDD) plots reveals distinct interaction mechanisms between the Fe-MoS_2 monolayer and the adsorbed gas molecules (CO, H_2S, and NO_2) (Fig. 5). Quantitatively, the computed charge transfer from the gas molecules to the substrate was approximately +0.011 *e* (CO), −0.0191 *e* (H_2S), and +0.0178 *e* (NO_2), respectively, where positive values denote electron transfer to the substrate.

For the CO-adsorbed system, a slight electron donation to the substrate was observed, suggesting moderate orbital hybridization, particularly involving the Fe-3d and CO-2π orbitals. This is consistent with the moderate adsorption energy (−1.8 eV) and implies a predominantly physisorption-driven interaction, with minor charge polarization effects. In contrast, H_2S exhibited a net charge transfer away from the substrate (−0.0191 *e*), indicating that the gas molecule acts as a weak electron acceptor. This result aligns with the positive adsorption energy (+2.5 eV), confirming the thermodynamic instability of H_2S adsorption on the Fe-MoS_2 surface. The minimal charge redistribution observed in the CDD further supports the conclusion that H_2S only weakly perturbs the electronic structure of the host material.

For the NO_2-adsorbed configuration, the substrate gains a small amount of charge (+0.0178 *e*), which may be attributed to the high electron affinity of NO_2 and the potential formation of partial charge transfer complexes. The corresponding

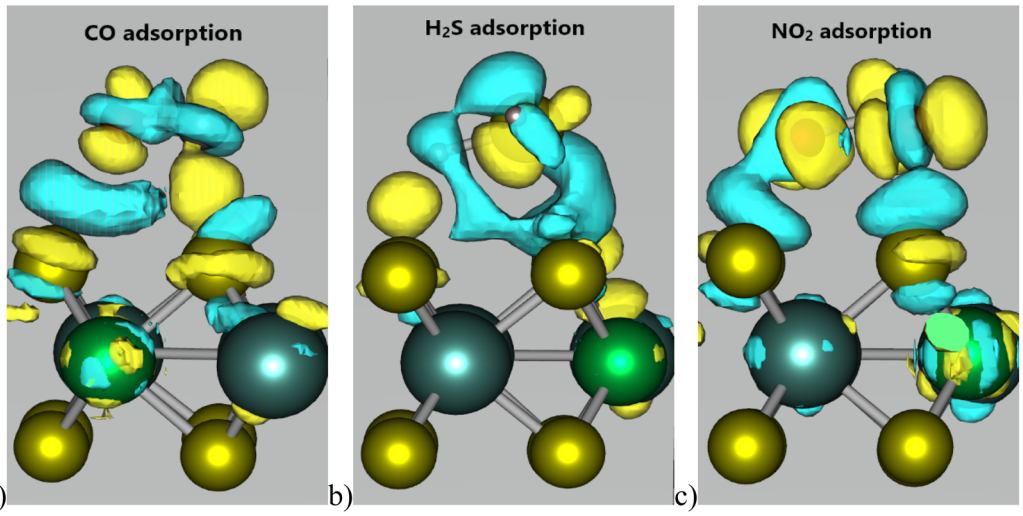

Fig. 5 Charge density difference in adsorbed configurations (the yellow and blue regions represent increases and decreases in charge, respectively): CO adsorption (a), H_2S adsorption (b), NO_2 adsorption (c).

adsorption energy (−1.6 eV) and visible charge accumulation around the adsorption site suggest stronger physisorption or weak chemisorption. Notably, the electron density rearrangement also contributes to the observed suppression of magnetic moments in this configuration. The low magnitude of charge transfer (<0.02 *e* in all cases) indicates that the interactions between gas molecules and Fe-MoS_2 are primarily governed by weak van der Waals forces and electrostatic polarization, rather than strong covalent bonding. These findings are in good agreement with the electronic and magnetic properties discussed in subsequent sections.

The Joint Density of States (JDOS) serves as a fundamental quantity for assessing the optical absorption characteristics, electron–hole pair generation, and modifications in electronic structure under the influence of electromagnetic radiation. Fig. 6 presents the calculated JDOS for the pristine Fe-MoS_2 monolayer and for three gas-adsorbed configurations: CO, H_2S, and NO_2. The results indicate that, within the low-energy photon range ($\hbar\omega$ < 9 eV), the JDOS profiles of all configurations remain relatively similar, suggesting that the electronic states responsible for transitions in this region are not significantly perturbed by gas adsorption. This implies that the low-energy optical properties of the material are largely preserved across the different adsorption states.

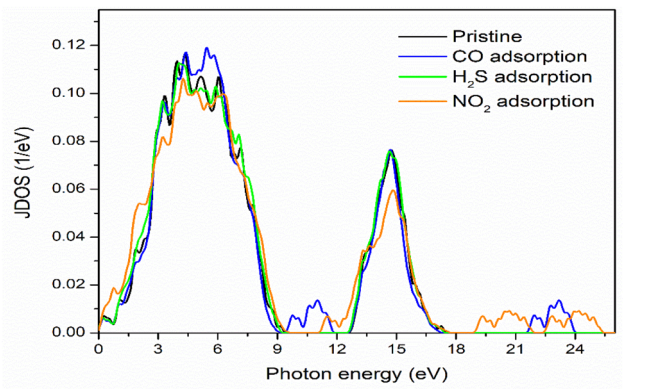

Fig. 6 Joint density of states (JDOS) of pristine Fe-MoS_2 monolayer structures and gas-adsorbed Fe-MoS_2 structures.

A key observation is the presence of non-zero JDOS values at very low photon energies, indicating the availability of accessible electronic states near the Fermi level that can participate in optical transitions even under low-energy excitation. This behavior is characteristic of semi-metallic systems and corroborates the findings from band structure analysis. Specifically, the pristine Fe-MoS_2, as well as the CO- and H_2S-adsorbed configurations, exhibit spin-polarized semi-metallic characteristics, while the NO_2-adsorbed system displays a fully metallic nature. The metallicity of the NO_2-adsorbed configuration facilitates continuous low-energy transitions, thereby enhancing its optical activity in the infrared-to-visible spectral range.

In the photon energy range of 3–7 eV, corresponding to the visible and near-ultraviolet (UV) regions, all configurations – including the pristine Fe-MoS_2 monolayer and the gas-adsorbed systems – exhibit pronounced Joint Density of States (JDOS) values. This indicates a high density of available electronic transitions, which directly correlates with efficient photon absorption in this spectral range. Such behavior confirms the suitability of Fe-MoS_2 systems, regardless of adsorption state, for optoelectronic applications such as photovoltaic devices and optical sensors operating in the visible – UV domain.

However, notable divergence between configurations emerges in the higher-energy range of 9–12 eV. While the pristine, H_2S-adsorbed, and NO_2-adsorbed structures exhibit JDOS values that remain close to zero – indicating a lack of accessible transitions – distinct features appear in the CO-adsorbed configuration. Specifically, several small peaks are observed, suggesting the activation of new high-energy optical transitions. This phenomenon is likely associated with strong orbital

hybridization between CO molecular states, particularly O(2p), and Fe/S atomic states, which gives rise to defect-like or mid-gap states within this energy range.

In the deep ultraviolet region (19–25.5 eV), a similar pattern is observed. Only the NO_2-adsorbed configuration presents multiple JDOS peaks, whereas the pristine and H_2S-adsorbed systems display JDOS values that remain effectively zero throughout this range, indicating the absence of transition-active states. The emergence of these high-energy features in the NO_2 system signifies substantial perturbation of the electronic structure due to NO_2 adsorption, extending well beyond the vicinity of the Fermi level. The induced modifications enable additional intraband and interband transitions, which are characteristic of strong molecular hybridization and electronic asymmetry. Additionally, the CO-adsorbed system also exhibits non-zero JDOS values in the 21.7–24 eV range, though with a lower intensity and fewer peaks compared to the NO_2 configuration. This suggests a moderate influence of CO adsorption on high-energy electronic states.

3.3. Optical results

Fig. 7 shows the real part of the dielectric function, $\varepsilon_1(\omega)$, along the in-plane x and y crystallographic directions for the pristine Fe-MoS_2 monolayer and the gas-adsorbed configurations (CO, H_2S, and NO_2). As the primary descriptor of the material's polarization response under an external electric field, $\varepsilon_1(\omega)$ governs key optical behaviors such as refractive index, transmittance, and absorption.

For pristine Fe-MoS_2, $\varepsilon_1(\omega)$ along the x and y directions overlaps nearly perfectly throughout the full photon-energy range considered, indicating strong in-plane dielectric isotropy. This behavior is consistent with the intrinsic hexagonal symmetry and uniform electronic distribution within the basal plane of the monolayer. Upon adsorption of CO, H_2S, and NO_2, a slight but noticeable deviation emerges between the $\varepsilon_1(\omega)$ responses along the two crystallographic directions. Although the induced anisotropy remains modest, it clearly indicates a partial breaking of in-plane symmetry due to the localized electronic perturbation introduced by the adsorbed species. This demonstrates that gas adsorption modifies the polarization pathways of the substrate and introduces mild direction-dependent dielectric behavior.

Across all configurations, the first major peak in $\varepsilon_1(\omega)$ appears near 1 eV, falling within the near-infrared (NIR) region. This feature originates from low-energy interband transitions close to the Fermi level and is characteristic of two-dimensional semiconductors. Furthermore, $\varepsilon_1(\omega)$ maintains relatively high values across the 1–3 eV range, spanning the NIR and the lower visible spectrum. A large real dielectric response in this region reflects strong material polarization and the associated attenuation of internal electric fields, often referred to as optical shielding. This suggests that Fe-MoS_2 efficiently reflects or absorbs incident light in this spectral window, consistent with behaviors typically exploited in photodetection or optical-filtering contexts.

At higher photon energies (3–8 eV), corresponding to the near-UV to mid-UV range, $\varepsilon_1(\omega)$ decreases sharply, indicating

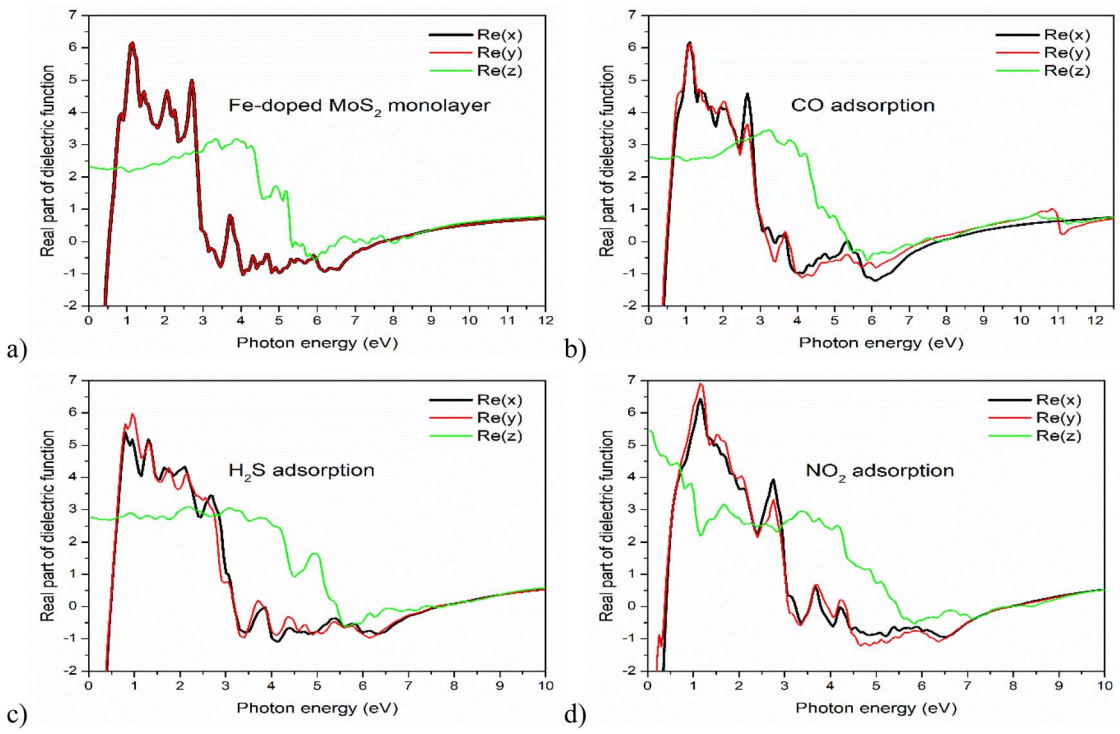

Fig. 7 Real part of dielectric function of the pristine Fe-MoS_2 monolayer structure (a) and the Fe-MoS_2 monolayer structures adsorbed with gases: CO (b), H_2S (c), NO_2 (d).

suppression of low-energy polarizable transitions and increased optical transparency. Beyond ~10 eV, $\varepsilon_1(\omega)$ approaches a nearly constant baseline, consistent with dielectric saturation and the dominance of transitions from deeper core states. This asymptotic response is characteristic of inertial, weakly dispersive dielectric behavior at very high excitation energies. The curves corresponding to the gas molecules serve only as complementary information to illustrate how adsorption perturbs the optical response of F-MoS_2 monolayer.

Fig. 8 presents the imaginary part of the dielectric function, $\varepsilon_2(\omega)$, for pristine Fe-MoS_2 and the gas-adsorbed configurations (CO, H_2S, and NO_2). Since $\varepsilon_2(\omega)$ quantifies the material's dissipative response to incident electromagnetic radiation, it is directly linked to the probability of optical absorption arising from interband electronic transitions. In this subsection, our discussion focuses primarily on how adsorption modifies the optical response of the Fe-MoS_2 monolayer; the spectra associated with the adsorbed molecules are included as complementary information to illustrate their perturbative effects on the substrate.

For the pristine Fe-MoS_2 monolayer, the $\varepsilon_2(\omega)$ curves along the x and y directions overlap exactly across the entire photon-energy range, reflecting the strong in-plane optical isotropy expected from a two-dimensional system with high structural symmetry. This uniformity indicates that optical transitions in the pristine configuration do not favor any crystallographic direction, consistent with a homogeneous charge distribution throughout the basal plane.

Gas adsorption leads to a modest divergence between the x- and y-direction $\varepsilon_2(\omega)$ spectra, particularly within selected low- and mid-energy regions. Although the induced anisotropy remains small, it reflects a partial breakdown of the in-plane symmetry caused by local electronic rearrangements at the adsorption site. The interaction between the adsorbed molecules and the Fe-MoS_2 lattice perturbs the orbital hybridization near the Fermi level, producing slight direction-dependent modifications to the optical absorption profile. Nevertheless, the overall magnitude of this anisotropy is limited, indicating that Fe-MoS_2 retains an essentially isotropic dissipative response even after adsorption-consistent with the trends observed in the real dielectric component $\varepsilon_1(\omega)$.

A key spectral feature across all configurations is the pronounced absorption peak in $\varepsilon_2(\omega)$ centered around ~3 eV, which lies in the visible range. This peak arises from strong interband transitions between occupied valence-band states and low-lying conduction-band states. Its persistence across all gas-adsorption scenarios shows that the fundamental optical absorption mechanism of Fe-MoS_2 remains intact, with the adsorbed molecules acting only as perturbations rather than fundamentally altering the intrinsic transition channels of the monolayer.

At higher photon energies (>8.5 eV), within the deep ultraviolet (DUV) regime, $\varepsilon_2(\omega)$ rapidly decays toward near-zero values. This decline reflects the limited availability of accessible unoccupied states at these high energies and the suppression of dipole-allowed transitions. As a result, the system becomes largely transparent to DUV radiation and

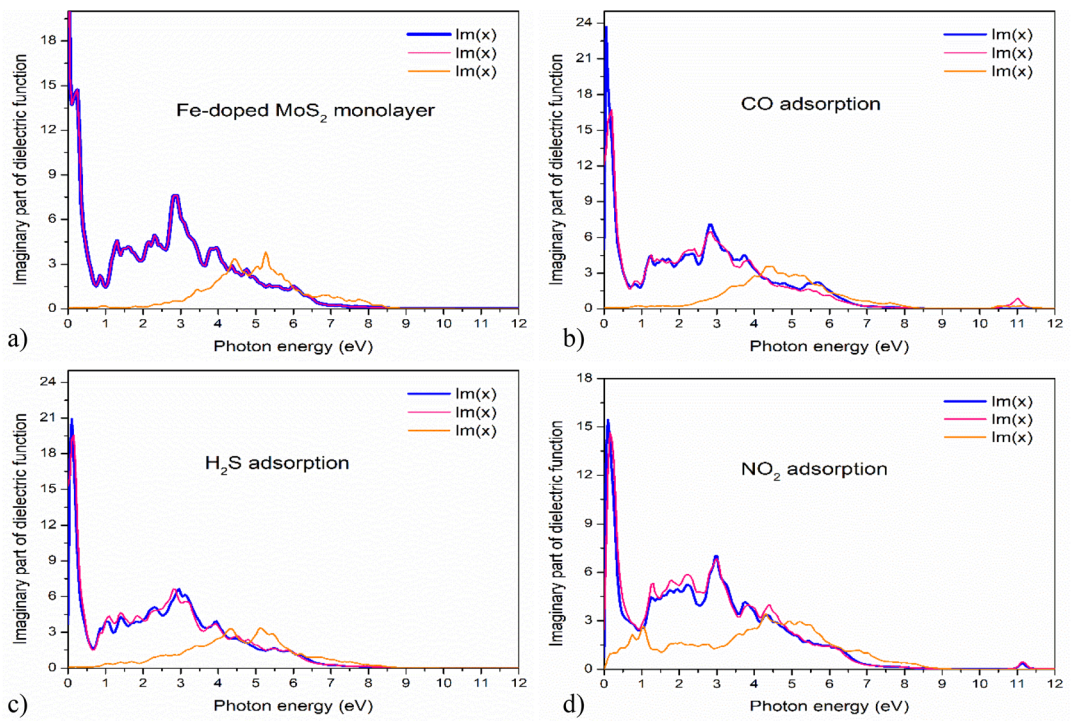

Fig. 8 Imaginary part of dielectric function of the pristine Fe-MoS_2 monolayer structure (a) and the Fe-MoS_2 monolayer structures adsorbed with gases: CO (b), H_2S (c), NO_2 (d).

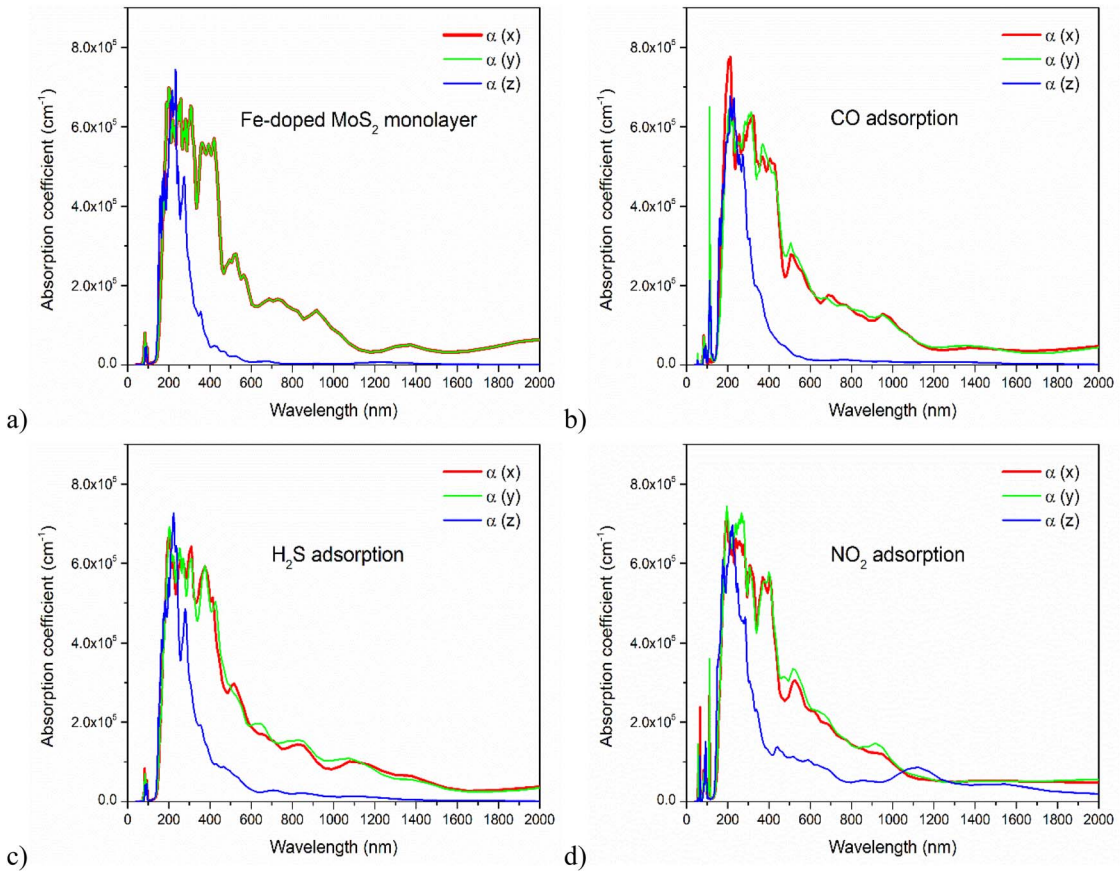

Fig. 9 Absorption coefficient of the pristine Fe-MoS_2 monolayer structure (a) and the Fe-MoS_2 monolayer structures adsorbed with gases: CO (b), H_2S (c), NO_2 (d).

exhibits minimal energy dissipation through absorption. This behavior is consistent across all configurations and underscores the intrinsic inertial, weakly dispersive nature of Fe-MoS_2 at high excitation energies.

Fig. 9 shows the optical absorption coefficient, $\alpha(\omega)$, for pristine Fe-MoS_2 and the gas-adsorbed configurations (CO, H_2S, and NO_2) along the three principal crystallographic directions. As $\alpha(\omega)$ reflects the material's ability to attenuate incident light through interband transitions, these spectra allow us to assess how gas adsorption perturbs the intrinsic optical response of the Fe-MoS_2 monolayer. Across all configurations, the strongest absorption occurs in the 200–500 nm wavelength range, covering the near-ultraviolet (NUV) and the entire visible region. This prominent absorption arises from efficient interband transitions involving states near the Fermi level, and its persistence in both pristine and adsorbed structures indicates that the fundamental optical activity of Fe-MoS_2 remains intact despite adsorption. These trends characterize the spectral regime where the monolayer intrinsically exhibits strong light–matter interaction, providing a baseline for understanding how external perturbations such as gas adsorption modulate the optical performance.

At wavelengths longer than ~500 nm, $\alpha(\omega)$ decreases rapidly for all configurations. In the out-of-plane (z) direction – perpendicular to the monolayer surface – the absorption drops sharply beyond 300 nm and approaches nearly zero for the pristine, CO-adsorbed, and H_2S-adsorbed systems. This behavior is characteristic of two-dimensional materials, in which optically active states are largely confined within the xy-plane. Due to limited orbital overlap and weak electronic dispersion along the z-axis, optical transitions in this direction are strongly suppressed, resulting in minimal absorption.

A notable deviation from this trend occurs for the NO_2-adsorbed configuration. Although $\alpha(\omega)$ in the z direction still decreases at longer wavelengths, it remains finite instead of vanishing. This behavior signifies partial breaking of out-of-plane symmetry and can be attributed to the stronger electronic interaction between NO_2 and the Fe-MoS_2 substrate. The associated charge redistribution and enhanced orbital hybridization introduce small but active electronic states with out-of-plane character, enabling weak absorption perpendicular to the monolayer surface. It demonstrates that adsorption can subtly tune vertical optical responses in Fe-MoS_2, an effect that may be useful in understanding interlayer coupling or out-of-plane optical behavior in more complex stacked or heterostructured systems.

4. Conclusions

In this study, the structural, electronic, thermo-mechanical, and optical properties of Fe-doped monolayer MoS_2 (Fe-MoS_2)

were systematically investigated in both pristine form and in the presence of adsorbed CO, H_2S, and NO_2 molecules, employing DFT in combination with a Crystal Graph Convolutional Neural Network (CGCNN) machine-learning framework. The adsorption analysis reveals that CO and NO_2 exhibit negative adsorption energies, indicating thermodynamically favorable interactions with the Fe-MoS_2 surface, whereas H_2S shows a positive adsorption energy, signifying an energetically unfavorable adsorption process under the considered conditions. These distinctions highlight the differing adsorption behaviors among the gas species and their varying impacts on the physicochemical properties of Fe-MoS_2.

Electronic structure analysis revealed that the pristine, CO-, and H_2S-adsorbed Fe-MoS_2 systems preserved a spin-polarized semimetallic character, whereas NO_2 adsorption induced a transition to metallic behavior and significantly suppressed the magnetic moment. The projected density of states (PDOS) and charge density difference (CDD) analyses indicated substantial charge redistribution upon adsorption, highlighting distinct charge transfer mechanisms and hybridization patterns depending on the adsorbed gas species.

Thermo-mechanical evaluations demonstrated anisotropic mechanical responses to gas adsorption: CO and NO_2 enhanced the bulk modulus, suggesting increased stiffness, while H_2S caused a marked reduction in shear modulus, indicative of localized lattice softening. Thermal properties – including isochoric/isentropic heat capacities, Debye temperature, and thermal expansion coefficient – remained relatively stable across configurations, confirming thermal robustness of the system post-adsorption.

Optical analysis, including the real and imaginary parts of the dielectric function, absorption coefficient, and joint density of states (JDOS), confirmed strong light absorption in the 200–500 nm spectral range (UV-visible), with retained or tunable optical activity after gas adsorption. JDOS results corroborated the presence of high transition state densities in the visible-UV region, with selective enhancement at high energies depending on the gas species.

Overall, the results suggest that Fe-MoS_2 monolayers show potential for selective gas detection toward specific molecules such as CO and NO_2, in addition to 2D optoelectronic applications. The unfavorable adsorption of H_2S further emphasizes the selective nature of the gas detection response, indicating that this material may not be suitable for all gas species.

Author contributions

N. V. Hoang researched, surveyed and set up input files. Tr. Q. Trieu prepared the figures, the tables. N. V. Hoang and Tr. Q. Trieu wrote the main manuscript. All authors reviewed the manuscript.

Conflicts of interest

We declare we have no competing interests.

Data availability

Data supporting the findings of this study are available within the article.

Acknowledgements

The authors gratefully acknowledge the support of the HPC system at the Institute for Advanced Study in Technology (IAST), Ton Duc Thang University.

References

1 S. Huang, *et al.*, Significant enhancement in thermoelectric performance of Mg_3Sb_2 from bulk to two-dimensional mono layer, *Nano Energy*, 2019, **62**, 212–219.
2 B. Nourozi, *et al.*, The electronic and optical properties of MgO mono-layer: Based on GGA-mBJ, *Results Phys.*, 2019, **12**, 2038–2043.
3 J. Sun, *et al.*, Electronic, transport, and optical properties of bulk and mono-layer $PdSe_2$, *Appl. Phys. Lett.*, 2015, **107**, 153902.
4 M. Liu, *et al.*, Colloidal quantum dot electronics, *Nat. Electron.*, 2021, **4**(8), 548–558.
5 N. Roch, *et al.*, Quantum phase transition in a single-molecule quantum dot, *Nature*, 2008, **453**(7195), 633–637.
6 H. Van Ngoc and C. V. Ha, C, Ge-doped h-BN quantum dot for nano-optoelectronic applications, *J. Phys.: Condens. Matter*, 2024, **36**(19), 195701.
7 C.-C. Pan, *et al.*, High-power, low-efficiency-droop semipolar (2021) single-quantum-well blue light-emitting diodes, *Appl. Phys. Express*, 2012, **5**(6), 062103.
8 K. Wang, *et al.*, Lead-free organic–perovskite hybrid quantum wells for highly stable light-emitting diodes, *ACS Nano*, 2021, **15**(4), 6316–6325.
9 X. Zhao, *et al.*, Rational construction of staggered InGaN quantum wells for efficient yellow light-emitting diodes, *Appl. Phys. Lett.*, 2021, **118**, 182102.
10 Y. B. Cao, *et al.*, High-efficiency, flexible and large-area red/green/blue all-inorganic metal halide perovskite quantum wires-based light-emitting diodes, *Nat. Commun.*, 2023, **14**(1), 4611.
11 J.-P. Leburton, Optic-phonon-limited transport and anomalous carrier cooling in quantum-wire structures, in *Physical Models for Quantum Wires, Nanotubes, and Nanoribbons*, Jenny Stanford Publishing, 2023, pp. 229–249.
12 Y. Sato, *et al.*, Strong electron-electron interactions of a Tomonaga-Luttinger liquid observed in InAs quantum wires, *Phys. Rev. B*, 2019, **99**(15), 155304.
13 M. Chhowalla, *et al.*, The chemistry of two-dimensional layered transition metal dichalcogenide nanosheets, *Nat. Chem.*, 2013, **5**(4), 263–275.
14 A. Splendiani, *et al.*, Emerging photoluminescence in monolayer MoS_2, *Nano Lett.*, 2010, **10**(4), 1271–1275.
15 K. F. Mak, *et al.*, Atomically thin MoS_2: a new direct-gap semiconductor, *Phys. Rev. Lett.*, 2010, **105**(13), 136805.

16 B. Radisavljevic, *et al.*, Single-layer MoS_2 transistors, *Nat. Nanotechnol.*, 2011, **6**(3), 147–150.
17 H. Gao, *et al.*, Tuning electrical conductance of MoS_2 monolayers through substitutional doping, *Nano Lett.*, 2020, **20**(6), 4095–4101.
18 S. Mouri, Y. Miyauchi and K. Matsuda, Tunable photoluminescence of monolayer MoS_2 via chemical doping, *Nano Lett.*, 2013, **13**(12), 5944–5948.
19 J. Tang, *et al.*, In situ oxygen doping of monolayer MoS_2 for novel electronics, *Small*, 2020, **16**(42), 2004276.
20 B. Gao, *et al.*, Magnetic properties of Mn-doped monolayer MoS_2, *Phys. Lett. A*, 2021, **414**, 127636.
21 Y. Yao, D. Liu and W. Ding, Electronic and optical properties of Cr-Mn co-doped in monolayer MoS_2: A first-principles study, *Mater. Today Commun.*, 2024, **41**, 110754.
22 K. Prajakta, *et al.*, Effect of introducing defects and doping on different properties of monolayer MoS_2, *Phys. Status Solidi B*, 2023, **260**(9), 2300017.
23 X. Deng, *et al.*, Adsorption of formaldehyde on transition metal doped monolayer MoS_2: A DFT study, *Appl. Surf. Sci.*, 2019, **484**, 1244–1252.
24 P. Rastogi, *et al.*, Doping strategies for monolayer MoS_2 via surface adsorption: a systematic study, *J. Phys. Chem. C*, 2014, **118**(51), 30309–30314.
25 Y. Wang, *et al.*, First-principles study of transition-metal atoms adsorption on MoS_2 monolayer, *Phys. E*, 2014, **63**, 276–282.
26 S. Yang, *et al.*, A DFT study on the hydrogen storage performance of MoS_2 monolayers doped with group 8B transition metals, *Int. J. Hydrogen Energy*, 2021, **46**(47), 24233–24246.
27 L. Li, *et al.*, Nonmetal (B, C, N, O, F) doping regulates the electron distribution of monolayer MoS_2 for Hg^0 adsorption, *Surf. Sci.*, 2023, **736**, 122355.
28 R. Albaridy, *et al.*, Strain-induced sulfur vacancies in monolayer MoS_2, *ACS Mater. Lett.*, 2023, **5**(9), 2584–2593.
29 W. Jia-Xin, *et al.*, Effect of tensile and compressive strains on the electronic structure of O-atom-doped monolayer MoS_2, *Int. J. Mod. Phys. B*, 2025, **39**(01), 2550012.
30 W. Jiang, *et al.*, Strain-Engineered Anisotropic Thermal Transport in Layered MoS_2 Structures, *ACS Appl. Mater. Interfaces*, 2025, **17**, 34833–34844.
31 H. Shin, *et al.*, Nonconventional strain engineering for uniform biaxial tensile strain in MoS_2 thin film transistors, *ACS Nano*, 2024, **18**(5), 4414–4423.
32 J. Sivek, H. Sahin, B. Partoens and F. M. Peeters, Adsorption and absorption of boron, nitrogen, aluminum, and phosphorus on silicene: stability and electronic and phonon properties, *Phys. Rev. B: Condens. Matter Mater. Phys.*, 2013, **87**, 085444.
33 J.-N. Yuan, *et al.*, First-principles study of electronic and elastic properties of hexagonal layered crystal MoS_2 under pressure, *Z. Naturforsch., A: Phys. Sci.*, 2015, **70**(7), 529–537.
34 X. Hu, *et al.*, Mapping thermal expansion coefficients in freestanding 2D materials at the nanometer scale, *Phys. Rev. Lett.*, 2018, **120**(5), 055902.
35 Q. Yue, *et al.*, Adsorption of gas molecules on monolayer MoS_2 and effect of applied electric field, *Nanoscale Res. Lett.*, 2013, **8**(1), 425.
36 H. Wei, *et al.*, A DFT study on the adsorption of H_2S and SO_2 on Ni doped MoS_2 monolayer, *Nanomaterials*, 2018, **8**(9), 646.
37 Y. Linghu and C. Wu, Gas molecules on defective and nonmetal-doped MoS_2 monolayers, *J. Phys. Chem. C*, 2019, **124**(2), 1511–1522.
38 M. P. K. Sahoo, *et al.*, Modulation of gas adsorption and magnetic properties of monolayer-MoS_2 by antisite defect and strain, *J. Phys. Chem. C*, 2016, **120**(26), 14113–14121.
39 M. J. Szary and P. Radomski, Unveiling the chemical underpinnings behind the enhanced adsorption interaction of NO_2 on MoS_2, $MoSe_2$, and $MoTe_2$ transition metal dichalcogenides, *J. Phys. Chem. C*, 2023, **127**(43), 21374–21386.